Table 2.7.4.1. *Monolithic monochromator for plane-wave synchrotron-radiation topography*

Reflection 1	$\bar{3}33$
Reflection 2	$\bar{1}3\bar{1}$
Reflection 3	$1\bar{3}\bar{1}$
Output wavelength	0.12378 nm
Spectral pass band, $d\lambda/\lambda$	$\sim 7 \times 10^{-6}$
Angular divergence of exit beam	$\sim 1.4 \times 10^{-6}$
Size of exit beam	15×15 mm

incident on the specimen crystal, the three crystals together forming a $+ + -$ arrangement (Ishikawa, Kitano & Matsui, 1985). The first monochromator is oriented for asymmetric $11\bar{1}$ Bragg reflection, the second for highly asymmetric $55\bar{3}$ reflection ($W_{out}/W_{in} = 64$ at $\lambda = 0.12$ nm), resulting in a divergence of only 0.5×10^{-6} in the beam impinging on the specimen.

Multireflection systems, some of which were proposed by Du Mond (1937) but not at that time realizable, have become a practicality through the advent of perfect silicon and germanium. When multiple reflection occurs between the walls of a channel cut in a perfect crystal, the tails of the curve of angular dependence of reflection intensity can be greatly attenuated without much loss of reflectivity at the peak of the curve (Bonse & Hart, 1965*a*). Beaumont & Hart (1974) described combinations of such 'channel-cut' monochromators that were suitable for use with synchrotron sources. One combination, consisting of a pair of contra-rotating channel-cut crystals, with each channel acting as a pair of reflecting surfaces in symmetrical $+ -$ setting, has found much favour as a monochromatizing device producing neither angular deviation nor spatial displacement of the final beam, whatever the wavelength it is set to pass. The properties of monoliths with one or more channels and employing two or more asymmetric reflections in succession have been analysed by Kikuta & Kohra (1970), Kikuta (1971), and Matsushita, Kikuta & Kohra (1971).

Symmetric channel-cut monochromators in perfect undistorted crystals transmit harmonic reflections. Several approaches to the problem of harmonic elimination may be taken, such as one of the following procedures (or possibly more than one in combination).

(1) Using crystals of slightly different interplanar spacing (*e.g.* silicon and germanium) in the $+ -$ setting, which then becomes slightly dispersive (Bonse, Materlik & Schröder, 1976; Bauspiess, Bonse, Graeff & Rauch, 1977).

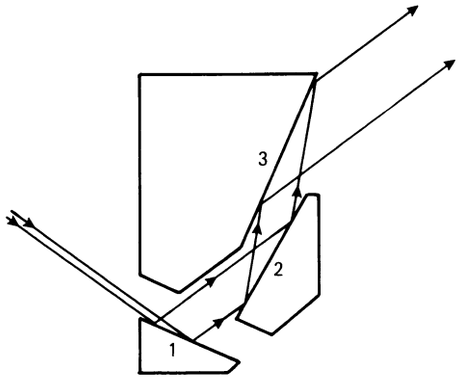

Fig. 2.7.4.1. Monolithic multiply reflecting monochromator for plane-wave topography.

(2) Laue case (transmission) followed by Bragg case (reflection), with deliberate slight misorientation between the diffracting elements (Materlik & Kostroun, 1980).

(3) Asymmetric reflection in non-parallel channel walls in a monolith (Hashizume, 1983).

(4) Misorientating a multiply reflecting channel, either one wall with respect to the opposite wall, or one length segment with respect to a following length segment (Hart & Rodrigues, 1978; Bonse, Olthoff-Münter & Rumpf, 1983; Hart, Rodrigues & Siddons, 1984).

For X-ray topographic applications, it is very desirable to have a spatially wide beam issuing from the multiply reflecting device. This is achieved, together with small angular divergence and spectral window, and without need of mechanical bending, in a monolith design by Hashizume, though it lacks wavelength tunability (Petroff, Sauvage, Riglet & Hashizume, 1980). The configuration of reflecting surfaces of this monolith is shown in Fig. 2.7.4.1. Reflection occurs in succession at surfaces 1, 2, and 3. The monochromator characteristics are listed in Table 2.7.4.1. The wavelength is very suitable in many topographic applications, and this design has proved to be an effective beam conditioner for use in synchrotron-radiation 'plane-wave' topography.

2.7.5. Some special techniques

2.7.5.1. *Moiré topography*

In X-ray optics, the same basic geometrical interpretation of moiré patterns applies as in light and electron optics. Suppose radiation passes successively through two periodic media, (1) and (2), whose reciprocal vectors are $\mathbf{h}_1$ and $\mathbf{h}_2$, so as to form a moiré pattern. Then, the reciprocal vector of the moiré fringes will be $\mathbf{H} = \mathbf{h}_1 - \mathbf{h}_2$. The magnitude, D, of the moiré fringe spacing is $|\mathbf{H}|^{-1}$ and may typically lie in the range 0.1 to 1 mm in the case of X-ray moiré patterns. Simple special cases are the 'rotation' moiré pattern in which $|\mathbf{h}_1| = |\mathbf{h}_2| = d^{-1}$, but $\mathbf{h}_1$ makes a small angle α with $\mathbf{h}_2$. Then, the spacing of the moiré fringes is d/α and the fringes run parallel to the bisector of the small angle α. The other special case is the 'compression' moiré pattern. Here, $\mathbf{h}_1$ and $\mathbf{h}_2$ are parallel but there is a small difference between their corresponding spacings, d_1 and d_2. The spacing D of compression moiré fringes is given by $D = d_1 d_2/(d_1 - d_2)$ and the fringes lie parallel to the grating rulings or Bragg planes in (1) and (2). X-ray moiré topographs achieve sensitivities of 10^{-7} to 10^{-8} in measuring orientation differences or relative differences in interplanar spacing. Moreover, if either periodic medium contains a lattice dislocation, Burgers vector $\mathbf{b}$, for which $\mathbf{b} \cdot \mathbf{h} \neq 0$, then a magnified image of the dislocation will appear in the moiré pattern, as one or more fringes terminating at the position of the dislocation, the number of terminating fringes being $\mathbf{b} \cdot \mathbf{h}$, which is necessarily integral (Hashimoto & Uyeda, 1957).

X-ray moiré topography has been performed with two quite different arrangements, the Bonse & Hart interferometer, and by superposition of separate crystals (Brádler & Lang, 1968). For accounts of the principles and applications of the interferometer, see, for example, Bonse & Hart (1965*b*, 1966), Hart (1968, 1975*b*), Bonse & Graeff (1977), Section 4.2.6 and §4.2.6.3.1. Fig. 2.7.5.1 shows the arrangement (Hart, 1968, 1972) for obtaining large-area moiré topographs by traversing the interferometer relative to a ribbon incident beam in similar fashion to taking a normal projection topograph (Fig. 2.7.2.2); P is the incident-beam slit, Q is a

stationary slit selecting the beam that it is desired to record, and film, *F*, and interferometer, *SMA*, together traverse to and fro as indicated by the double-headed arrow. In Fig. 2.7.5.1, *S*, *M*, and *A* are the three equally thick wafers of the interferometer that remain upstanding above the base of the monolithic interferometer after the gaps between *S* and *M*, and *M* and *A*, have been milled away. The elements *S*, *M* and *A* are called the splitter, mirror, and analyser, respectively. The moiré pattern is formed between the Bragg planes of *A* and the standing-wave pattern in the overlapping $\mathbf{K}_0$ and $\mathbf{K}_h$ beams entering it. Maximum fringe visibility occurs in the emerging beam that the slit *Q* is shown selecting. A dislocation will appear in the moiré pattern whether the lattice dislocation lies in *S*, *M*, or *A*, provided $\mathbf{b} \cdot \mathbf{h} \neq 0$. Moiré patterns formed in a number of Bragg reflections whose normals lie in, or not greatly inclined to, the plane of the wafers, can be recorded by appropriate orientation of the monolith. By this means, it is easily discovered in which wafer the dislocation lies, and its Burgers vector can be completely determined, including its sense, the latter being found by a deliberate slight elastic deformation of the interferometer (Hart, 1972). Satisfactory moiré topographs have been obtained with an interferometer in a synchrotron beam, despite thermal gradients due to the local intense irradiation (Hart, Sauvage & Siddons, 1980).

Fig. 2.7.5.2 shows crystal slices (1), *ABCD*, and (2), *EFGH*, superposed and simultaneously Bragg reflecting in the Brádler–Lang (1968) method of X-ray moiré topography. The slices could have been cut from separate crystals. In the case when the Bragg planes of (1) and (2) are in identical orientation but have a translational mismatch across *CD* and *EF* with a component parallel to **h**, strong scattering occurs towards *Z* as focus, producing extra intensity at T' in the $\mathbf{K}_0$ beam TT'' and at R' in the $\mathbf{K}_h$ beam RR''. It is usual to record the moiré pattern using the $\mathbf{K}_h$ beam. Projection moiré topographs are obtained by the standard procedure of traversing the crystal pair and film together with respect to the incident beam *SO*. The special procedure devised for mutually aligning the two crystals so that $\mathbf{h}_1$ and $\mathbf{h}_2$ coincide within their angular range of reflection is explained by Brádler & Lang (1968). This method has been applied to silicon and to natural (Lang, 1968) and synthetic quartz (Lang, 1978).

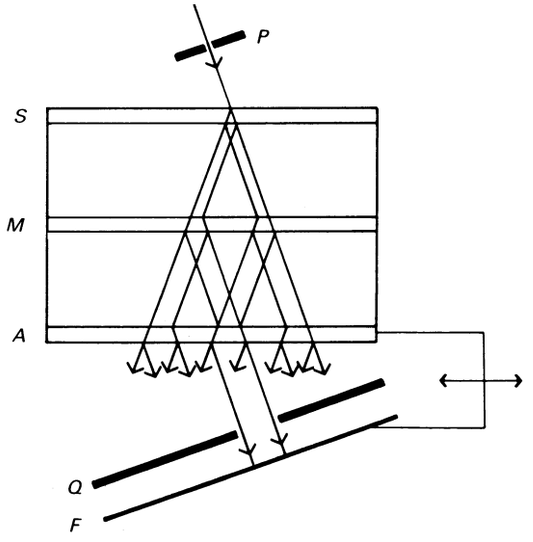

Fig. 2.7.5.1. Scanning arrangement for moiré topography with the Bonse–Hart interferometer.

2.7.5.2. *Real-time viewing of topograph images*

Position-sensitive detectors involving the production of electrons are described in Chapter 7.1, Sections 7.1.6 and 7.1.7, and Arndt (1986, 1990). Those descriptions cover all the image-forming devices that form the core of systems set up for 'live' X-ray topography. Here, discussion is limited to remarks on the historical development of techniques designed for making X-ray topographic images directly visible, and on the leading systems that are now sufficiently developed to be acceptable for routine use, in particular on topograph cameras set up at synchrotron X-ray sources. Two types of system became practicalities about the same time, that using direct conversion of X-rays to electronic signals by means of an X-ray-sensitive vidicon television camera tube (Chikawa & Fujimoto, 1968), and the indirect method using an external X-ray phosphor coupled to a multistage electronic image-intensifier tube (Reifsnider & Green, 1968; Lang & Reifsnider, 1969) or to a television-camera tube incorporating an image-intensifier stage (Meieran, Landre & O'Hara, 1969). These two approaches, the direct and the indirect, remain in competition. Developments up to the middle 1970's have been comprehensively reviewed by Hartman (1977). Since that time, Si-based, two-dimensional CCD (charge-coupled device) arrays have come into prominence as radiation detectors. They can be used for direct conversion of low-energy X-rays into electronic charges as well as for recording images of phosphor screens. As illustrated by Allinson (1994), four configurations employing CCD arrays for X-ray imaging can be considered: (i) direct detection by the 'naked' device; (ii) detection by phosphor coated directly on the CCD array; (iii) phosphor separate, and optically coupled to the CCD by lens or fibre-optics; and (iv) the addition to (iii) of an image intensifier

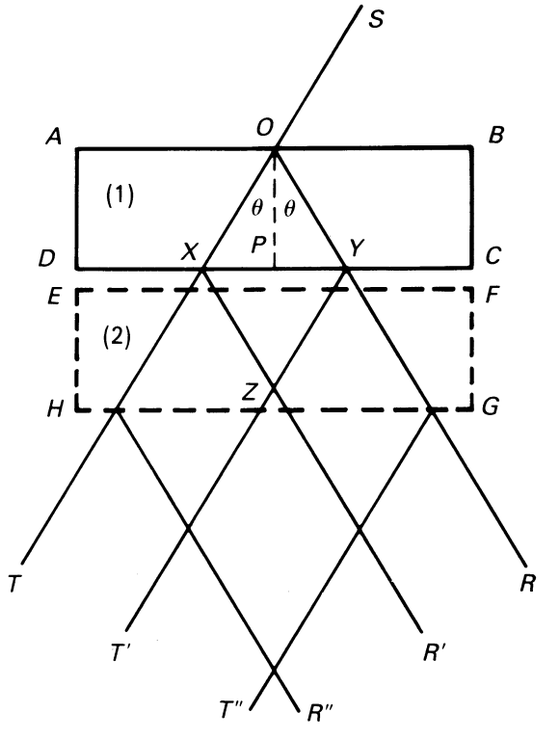

Fig. 2.7.5.2. Superposition of crystals (1) and (2) for production of moiré topographs. [Reproduced from *Diffraction and Imaging Techniques in Material Science*, Vol. II. *Imaging and Diffraction Techniques*, edited by S. Amelinckx, R. Gevers & J. Van Landuyt (1978), Fig. 21, p. 695. Amsterdam, New York, Oxford: North-Holland.]

or microchannel plate coupled to the phosphor screen. Consider first configuration (i). X-ray absorption efficiency in the active layer of silicon is near unity for radiations such as Cu $K\alpha$, and is not less than about 20% for Mo $K\alpha$ or Ag $K\alpha$. Since about one-third of the absorbed energy goes into electron–hole pair production, an absorbed 8 keV X-ray photon creates about 2000 pairs, a large number compared with a combined dark-current plus read-out noise level per photosite of a few tens of electrons r.m.s. Thus, single-photon counting is possible. Moreover, a cooled CCD can integrate the charge accumulated in each pixel for up to $\sim 10^3$ s. With pixel sizes in the range 10 to 30 μm square, and 1024×1024 (or 2048×2048) arrays in production, sensitive areas of 50 mm square, or greater, are available, sufficient for the majority of topographic applications.

For X-ray-sensitive TV-camera tubes, some major improvements in resolution and sensitivity have taken place since the first applications to X-ray topography of Be-windowed vidicons. Using the more sensitive 'Saticon' tube with incorporation of a 20 μm-thick Se–As target that provides good X-ray absorption efficiency, Chikawa, Sato & Fujimoto (1984) achieved a resolution as good as 6 μm at a modulation transfer function (MTF) of 5%. This betters that achieved with indirect systems or with standard-pixel-size CCD arrays used as direct detectors. The newer 'Harp' tube, which employs avalanche multiplication produced by a high field ($\sim 10^8$ V m^{-1}) applied across a 2 μm Se target to increase light sensitivity at least ten fold compared with the Saticon tube, has also been modified into a direct X-ray detector. Increasing the target thickness to 8 μm and adding an X-ray-transparent window provides satisfactory detector efficiency over a useful wavelength range (and the Se $K\alpha$-absorption edge at 0.098 nm causes absorption efficiencies for Cu $K\alpha$ and Mo $K\alpha$ to be similar, about 25%). The gain is sufficient for detection of single Cu $K\alpha$ photon-absorption events (at least for photons absorbed close to the target front, giving the maximum path for avalanche formation). A limiting resolution of about 25 μm (at MTF of ~33%) is exhibited (Sato, Maruyama, Goto, Fujimoto, Shidara, Kawamura, Hirai, Sakai & Chikawa, 1993), not yet as good as the 6 μm achieved with the Saticon tube. The rather small 6×9 mm sensitive areas of these camera tubes (when in standard '$\frac{2}{3}$ in' size) restricts their range of topographic applications as direct detectors compared with CCD arrays, but their amorphous Se targets are less likely to be degraded by X-radiation damage than crystalline-silicon CCD arrays. The latter do suffer degradation, but recover after treatment (Allinson, Allsopp, Quayle & Magorrian, 1991).

In the case of indirect systems, the lens or fibre-optic plate situated between phosphor and detector automatically protects the latter from radiation damage. Somewhat better resolution can be achieved by lens coupling than by fibre-optic coupling of phosphor to detector, but at the expense of loss of light-collection efficiency generally too great to be acceptable. In principle, magnification or de-magnification of the phosphor-screen image on the detector can be selected according to whether phosphor or detector has the better resolution, in order to maximize the system resolution as a whole. Phosphor resolution can be increased by diminishing its thickness below the value that would be chosen from consideration of X-ray absorption efficiency alone. Using a phosphor screen of Gd_2O_2S(Tb) only 5 μm thick, and lens-coupling it with tenfold magnification on to the target of a low-light-level television camera, Hartmann achieved a system resolution of about 10 μm (Queisser, Hartmann & Hagen, 1981), as good as any demonstrated so far with indirect systems.

The phosphors already used (or potentially usable) in real-time X-ray topography are inorganic compounds containing elements of medium or heavy atomic weight. They include ZnS(Ag), NaI(Tl), CsI(Tl), Y_2O_2S(Tb), Y_2O_2S(Eu), La_2O_2S(Eu) and Gd_2O_2S(Tb). Problems encountered are light loss by light trapping within single-crystal phosphor sheets, and resolution loss by light scattering from grain to grain in phosphor powders. Various ways of reducing lateral light-spreading within phosphor screens by imposing a columnar structure upon them have been tried. Most success has been achieved with CsI. Evaporated layers of this crystal have a natural tendency towards columnar cracking normal to the substrate. Then internal reflection within columns reduces 'cross talk' between columns (Stevels & Kühl, 1974). However, a columnar structure can be very effectively imposed on CsI films evaporated on to fibre-optic plates by etching away the cladding glass surrounding each fibre core to a depth of 10 μm, say. The evaporated CsI starts growing on the protruding cores, and continues as pillars physically separated and hence to a large degree optically separated from their neighbours (Ito, Yamaguchi & Oba, 1987; Allinson, 1994; Castelli, Allinson, Moon & Watson, 1994).

The drive to develop systems for 2D imaging of single-crystal or fibre diffraction patterns produced by synchrotron radiation that offer spatial resolution better than that within the grasp of position-sensitive multiwire gas proportional counters (say 100–200 μm) has produced several phosphor/fibre-optic/CCD combinations that with some modifications would be useful for real-time X-ray topography. Diffraction-pattern recording requires a sensitive area not less than about 50 mm in diameter, so most systems incorporate a fibre-optic taper to couple a larger phosphor screen with a small CCD array. Spatial resolution in the X-ray image cannot then be better than CCD pixel size multiplied by the taper ratio. In one system that has been fully described, this product is 20.5 μm × 2.6, and a point-spread FWHM of 80 μm on a 51×51 mm input area was realised without benefit from a columnar-structure phosphor (Tate, Eikenberry, Barna, Wall, Lawrance & Gruner, 1995). More appropriate for X-ray topography would be unit-magnification optical coupling of phosphor with a CCD array of not less than 1024×1024 elements and not more than 20 μm square pixel size. With such a combination, a system resolution of ~25 μm should be achievable; and at a synchrotron X-ray topography station at least one device offering resolution no worse than this should be available. There is a scope for both high-resolution, small-sensitive-area and lower-resolution, large-sensitive-area imaging systems in real-time X-ray topography. It has been shown possible to incorporate both types in a single topography camera for use with synchrotron radiation (Suzuki, Ando, Hayakawa, Nittono, Hashizume, Kishino & Kohra, 1984).

references